Journal of Computational Physics **172,** 704–717 (2001)
doi:10.1006/jcph.2001.6850, available online at http://www.idealibrary.com on IDEAL®

Lattice Boltzmann Equation on a Two-Dimensional Rectangular Grid

M'hamed Bouzidi,* Dominique d'Humières,*,† Pierre Lallemand,* and Li-Shi Luo‡

*Laboratoire C.N.R.S.-A.S.C.I., Bâtiment 506, Université Paris-Sud (Paris XI Orsay), 91405 Orsay Cedex, France; †Laboratoire de Physique Statistique de l'École Normale Supérieure, 24, Rue Lhomond, 75321 Paris Cedex 05, France; ‡ICASE, MS 132C, NASA Langley Research Center, 3 West Reid Street, Building 1152, Hampton, Virginia 23681-2199
E-mail: bouzidi@asci.fr; Dominique.Dhumieres@lps.ens.fr; lalleman@asci.fr; luo@icase.edu

Received January 4, 2001; revised May 23, 2001

We construct a multirelaxation lattice Boltzmann model [1] on a two-dimensional rectangular grid. The model is partly inspired by a previous work of Koelman [2] to construct a lattice BGK model on a two-dimensional rectangular grid. The linearized dispersion equation is analyzed to obtain the constraints on the isotropy of the transport coefficients and Galilean invariance for various wave propagations in the model. The linear stability of the model is also studied. The model is numerically tested for three cases: (a) a vortex moving with a constant velocity on a mesh with periodic boundary conditions; (b) Poiseuille flow with an arbitrary inclined angle with respect to the lattice orientation; and (c) a cylinder asymmetrically placed in a channel. The numerical results of these tests are compared with either analytic solutions or the results obtained by other methods. Satisfactory results are obtained for the numerical simulations.

1. INTRODUCTION

Historically originating from the lattice gas automata (LGA) introduced by Frisch, Hasslacher, and Pomeau [3], the lattice Boltzmann equation (LBE) has recently become an alternative method for computational fluid dynamics. The essential ingredients in any lattice Boltzmann models which are required to be completely specified are: (i) a discrete lattice space on which fluid particles reside; (ii) a set of discrete velocities (often going from one node to its nearest neighbors) to represent particle advection; and (iii) a set of rules for the redistribution of particles residing on a node to mimic collision processes in a real fluid. Fluid-boundary interactions are usually approximated by simple reflections of the particles by solid interfaces.

0021-9991/01 $35.00

In a hydrodynamic simulation by using the lattice Boltzmann equation, one solves the evolution equations of the distribution functions of fictitious fluid particles colliding and moving synchronously on a highly symmetric lattice space. The highly symmetric lattice space is a result of the discretization of particle velocity space and the condition for synchronous motions. That is, the discretizations of time and particle phase space are coherently coupled together. This makes the evolution of the lattice Boltzmann equation very simple—it consists of only two steps: collision and advection. One immediate limitation of the LBE method is due to its use of highly symmetric regular lattice mesh, which are usually triangular or square lattices in two dimensions and cubic in three dimensions. Obviously, this is a serious obstacle to its applications in many areas of computational fluid dynamics. To deal with complex computational domains, various proposals have been made to use grids that are better suited to fit boundaries or to adapt meshes according to the physics of the system.

It has been shown recently that the lattice Boltzmann equation is indeed a special finite difference form of the continuous Boltzmann equation with some drastic approximations tailored for hydrodynamic simulations [4, 5]. This makes the lattice Boltzmann method more amenable to incorporate body-fitted meshes [6] or grid refinement techniques [7]. In most cases, the regular lattice mesh is abandoned by decoupling the spatial–temporal discretizations and the discrete velocity set, so that interpolations can be used in addition to the advection on a nonregular or nonuniform mesh. However, interpolations introduce additional numerical viscosities and other artifacts into the lattice Boltzmann method [8]. Therefore, it is highly desirable to construct lattice Boltzmann models with arbitrary mesh and free of interpolations [2, 9].

In this paper, we shall consider a two-dimensional model on a rectangular grid with an aspect ratio of $a = \delta_y/\delta_x$, where $0 < a \leq 1$. The model is inspired in part by a previous work of Koelman [2] who proposed a general scheme to construct lattice BGK models with given discrete velocity sets based on a low Mach number expansion of the Maxwellian equilibrium distribution function. Conservation and symmetry constraints are imposed to fix the parameters in the equilibrium distribution function. Koelman's model is essentially a variation of the lattice BGK model [10, 11]. As we shall show, the transport coefficients of this model are generally anisotropic when $a \neq 1$ [12].

We use the generalized lattice Boltzmann equation with multiple relaxation times of d'Humières [1], instead of the standard lattice BGK model [10, 11]. The generalized LBE model has the freedom of multiple relaxations which can be independent or coupled together. This allows one to optimize the overall properties of the model through suitable compensation of inadequate behaviors. We shall study the time evolution of plane waves by analyzing the linearized dispersion equation of the model [8]. This analysis allows us to obtain the conditions under which the model can be used to simulate the Navier–Stokes equation, i.e., the model is Galilean invariant and isotropic up to a certain order in wave-number $\mathbf{k}$. We show that severe stability constraints are due to Galilean invariance and isotropy of transport coefficients. This demonstrates the difficulty in the endeavor of constructing a lattice Boltzmann model with arbitrary grid. Simulations of nontrivial cases are presented to demonstrate the qualities and defects of the model.

We organize the paper as follows. Section 2 describes the proposed model on a rectangular grid. Section 3 shows a detailed analysis of the dispersion equation. The wave-number dependence of Galilean coefficient and attenuation coefficients are computed explicitly to obtain the conditions under which the model is Galilean invariant and isotropic. Section 4 provides examples of numerical simulations using the proposed model: (a) a vortex moving

with a uniform velocity in a periodic system; (b) Poiseuille flow with the boundaries along arbitrary direction with respect to the underlying lattice; and (c) flow past a cylinder asymmetrically placed in a channel. Section 5 concludes the paper.

2. DEFINITION OF THE MODEL

We consider a two-dimensional LBE model with nine discrete velocities (the D2Q9 model) on a rectangular grid of dimensions 1 and a. (In what follows all quantities are given in nondimensional units, normalized by the lattice unit δ_x.) In the advection step of the lattice Boltzmann equation, particles move from one node of the grid to one of its neighbors as illustrated in Fig. 1. The discrete velocities are given by

$$\mathbf{e}_\alpha = \begin{cases} (0,\ 0)\,, & \alpha = 0, \\ (\cos[(\alpha-1)\pi/2],\ a\ \sin[(\alpha-1)\pi/2]), & \alpha = 1-4, \\ (\cos[(2\alpha-9)\pi/4],\ a\ \sin[(2\alpha-9)\pi/4])\sqrt{2}, & \alpha = 5-8, \end{cases} \tag{1}$$

where the duration of the time step δt is assumed to be unity. At any time t_n, the LBE fluid is then characterized by the populations of the nine velocities at each node of the computational domain

$$|\, f(\mathbf{r}_j,\ t_n)\rangle \equiv (\, f_0(\mathbf{r}_j,\ t_n),\ f_1(\mathbf{r}_j,\ t_n), \cdots,\ f_8(\mathbf{r}_j,\ t_n))^{\mathsf{T}}\,, \tag{2}$$

where T is the transpose operator. Here upon the Dirac notation of bra, $\langle\cdot|$, and ket, $|\cdot\rangle$, vectors is used to denote row column and row vectors, respectively. The time evolution of the state of the fluid follows the general equation

$$|\, f(\mathbf{r}_j + \mathbf{e}_\alpha,\ t_n + 1)\rangle = |\, f(\mathbf{r}_j,\ t_n)\rangle + |\Omega(\, f(\mathbf{r}_j,\ t_n))\rangle\,, \tag{3}$$

where collisions are symbolically represented by the operator Ω.

We shall use the generalized lattice Boltzmann equation introduced by d'Humières [1], in which the collision process is executed in moment space $\mathbb{M}$. The mapping between moment space and discrete velocity space $\mathbb{V}$ spanned by $\{\mathbf{e}_\alpha\}$ is one-to-one and defined by the linear

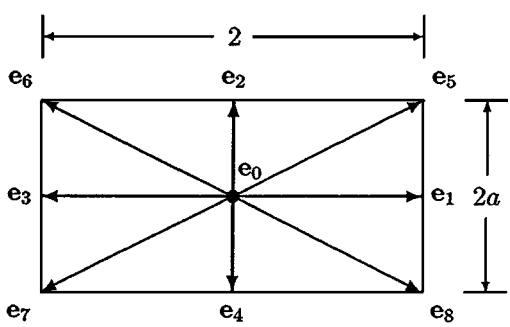

FIG. 1. Discrete velocities of the nine-velocity model on a rectangular grid. The aspect ratio of the rectangle is $\delta_y/\delta_x = a$.

transformation M which maps a vector $|f\rangle$ in $\mathbb{V}$ to a vector $|\hat{f}\rangle$ in $\mathbb{M}$, i.e.,

$$|\hat{f}\rangle = \mathsf{M}|f\rangle, \quad \text{and} \quad |f\rangle = \mathsf{M}^{-1}|\hat{f}\rangle. \tag{4}$$

To reflect the underlying symmetries appearing in both the Chapman–Enskog expansion and the dispersion equation, M is constructed as the following

$$\mathsf{M} = \begin{pmatrix} \langle m_1| \\ \langle m_2| \\ \langle m_3| \\ \langle m_4| \\ \langle m_5| \\ \langle m_6| \\ \langle m_7| \\ \langle m_8| \\ \langle m_9| \end{pmatrix} = \begin{pmatrix} 1 & 1 & 1 & 1 & 1 & 1 & 1 & 1 & 1 \\ -2\varphi_1 & \varphi_2 & \varphi_3 & \varphi_2 & \varphi_3 & \varphi_1 & \varphi_1 & \varphi_1 & \varphi_1 \\ 4 & -2 & -2 & -2 & -2 & 1 & 1 & 1 & 1 \\ 0 & 1 & 0 & -1 & 0 & 1 & -1 & -1 & 1 \\ 0 & -2 & 0 & 2 & 0 & 1 & -1 & -1 & 1 \\ 0 & 0 & a & 0 & -a & a & a & -a & -a \\ 0 & 0 & -2a & 0 & 2a & a & a & -a & -a \\ -2\varphi_4 & \varphi_5 & \varphi_6 & \varphi_5 & \varphi_6 & \varphi_4 & \varphi_4 & \varphi_4 & \varphi_4 \\ 0 & 0 & 0 & 0 & 0 & a & -a & a & -a \end{pmatrix} \tag{5}$$

$$= (|m_1\rangle,\ |m_2\rangle,\ |m_3\rangle,\ |m_4\rangle,\ |m_5\rangle,\ |m_6\rangle,\ |m_7\rangle,\ |m_8\rangle,\ |m_9\rangle)^{\mathsf{T}},$$

where $\varphi_1 = a^2 + 1$, $\varphi_2 = 1 - 2a^2$, $\varphi_3 = a^2 - 2$, $\varphi_4 = a^2 - 1$, $\varphi_5 = a^2 + 2$, and $\varphi_6 = -(1 + 2a^2)$.

The components of the row vector $\langle m_\beta|$ in matrix M are polynomials of the x and y components of the velocities $\{\mathbf{e}_\alpha\}$, $e_{\alpha,x}$ and $e_{\alpha,y}$. The vectors $\langle m_\beta|$, $\beta = 1, 2, \cdots, 9$, are orthogonalized by the Gram–Schmidt procedure in a carefully considered order. The first three orthogonal vectors correspond to the mass, x- and y-momentum modes: $\langle m_1| = \langle \|\mathbf{e}_\alpha\|^0|$, $\langle m_4| = \langle e_{\alpha,x}|$, and $\langle m_6| = \langle e_{\alpha,y}|$. The above expressions prescribe the components of $\langle m_1|$, $\langle m_4|$, and $\langle m_6|$. These three vectors span the hydrodynamic subspace of the eigenspace of the collision operator for a two-dimensional athermal LBE model. The remaining six vectors span the kinetic subspace. The vector $\langle m_2| = \langle 3\|\mathbf{e}_\alpha\|^2 - 2(1 + a^2)\|\mathbf{e}_\alpha\|^0|$ is constructed by orthogonalizing the energy mode $\langle \|\mathbf{e}_\alpha\|^2|$. Similarly, vectors $\langle m_5|$ and $\langle m_7|$ are respectively built upon $\langle e_{\alpha,x}\|\mathbf{e}_\alpha\|^2|$ and $\langle e_{\alpha,y}\|\mathbf{e}_\alpha\|^2|$; $\langle m_8|$ is constructed upon $\langle e_{\alpha,x}^2 - e_{\alpha,y}^2|$ and $\langle m_9| = \langle e_{\alpha,x}e_{\alpha,y}|$; and finally $\langle m_3|$ is obtained from $\langle \|\mathbf{e}_\alpha\|^4|$. By means of their construction, the row vectors in M are mutually orthogonal, but they are not normalized, their norms being chosen to simplify algebraic manipulations. When $a = 1$, M reduces to that for the D2Q9 model on a square grid with a different normalization of $|p_{xx}\rangle$ [8]. Therefore, the proposed model can be considered as a generalization of the model on a square lattice. It should be noted that when $a \neq 1$, there are three nonzero (kinetic) energy levels in the model which introduce additional degrees of freedom into the model and extra care must be taken in the construction of $\langle m_2|$, $\langle m_8|$, and $\langle m_3|$, i.e., they must be orthogonalized with the Gram–Schmidt procedure in the particular order of $\langle m_2|$, $\langle m_8|$, and $\langle m_3|$.

It is interesting to note that the moments $\langle m_\beta|f\rangle$ have a physical interpretation. The matrix M so constructed in the above naturally leads to the moment vector in moment space $\mathbb{M}$ as

$$|\hat{f}\rangle = (\rho,\ e,\ \varepsilon,\ j_x,\ q_x,\ j_y,\ q_y,\ p_{xx},\ p_{xy})^{\mathsf{T}}, \tag{6}$$

where ρ is the density, e is related to the kinetic energy, ε is related to the kinetic energy squared for $a = 1$ (but has no obvious physical meaning when $a \neq 1$), j_x and j_y are x

and y components of the momentum density, q_x and q_y are proportional to the x and y components of the energy flux, and p_{xx} and p_{xy} are proportional to the diagonal and off-diagonal components of the viscous stress tensor.

For the collision process, we propose to use the following equilibrium distribution functions of the (nonconserved) moments, which depend only on the conserved moments, i.e., ρ, and $\mathbf{j} = (j_x,\ j_y)$,

$$e^{(\mathrm{eq})} = 2\left(3c_s^2 - 1 - a^2\right)\rho + \frac{3}{\rho}\left(j_x^2 + j_y^2\right), \tag{7a}$$

$$\varepsilon^{(\mathrm{eq})} = \frac{1}{4}\alpha_3\rho, \tag{7b}$$

$$q_x^{(\mathrm{eq})} = \frac{1}{2}c_1 j_x, \tag{7c}$$

$$q_y^{(\mathrm{eq})} = \frac{1}{2}c_2 j_y, \tag{7d}$$

$$p_{xx}^{(\mathrm{eq})} = \frac{(a^2-1)}{a^2}\left[3(a^2+1)c_s^2 - 2a^2\right]\ \rho + \frac{3}{\rho}\left(a^2 j_x^2 - \frac{1}{a^2}j_y^2\right), \tag{7e}$$

$$p_{xy}^{(\mathrm{eq})} = \frac{1}{\rho}j_x j_y, \tag{7f}$$

where the coupling coefficient between $p_{xx}^{(\mathrm{eq})}$ and ρ (which vanishes in the standard D2Q9 LBE model) is introduced to obtain the isotropy of the sound speed. The values of the coupling constants (α_3, c_1, and c_2) in the above equilibria are obtained by optimizing isotropy and stability of the model [8]. It should be noted that the energy is not considered as a conserved quantity here because the model is athermal. (The model does not possess sufficient degrees of freedom to accommodate the dynamics of locally isotropic heat transport.)

In what follows the idea of the "incompressible" LBE [13] is applied to the above equilibria so that ρ is replaced by a constant ρ_0 in the denominators of equations (7a), (7e), and (7f). This choice allows for better comparison with other incompressible simulations and simpler algebra while retaining correct acoustics.

The collision process is modeled by the following relaxation equations

$$|\hat{f}^*\rangle = |\hat{f}\rangle - \mathsf{S}\left[|\hat{f}\rangle - |\hat{f}^{(\mathrm{eq})}\rangle\right], \tag{8}$$

where $|\hat{f}^*\rangle$ denotes the postcollision state, and S is the diagonal relaxation matrix

$$\mathsf{S} = \mathrm{diag}(0, s_2, s_3, 0, s_5, 0, s_7, s_8, s_9). \tag{9}$$

The model reduces to the usual lattice BGK model if all the relaxation parameters are set to be a single relaxation time τ (and $a = 1$), i.e., $s_\alpha = 1/\tau$. It should be stressed that the relaxation parameters are not independent, as shown in the next section. The constraints of isotropy lead to the coupling between these relaxation parameters [8]. Obviously, the usual lattice BGK model does not possess the freedom for such couplings, therefore it would not work on a rectangular grid.

3. ANALYSIS OF LINEARIZED DISPERSION EQUATION

The analysis presented in what follows is similar to that presented in [8], where the goal of the work was to determine the stability conditions for the coupling coefficients α_2 and α_3, and the constraints on the relaxation parameters s_α.

We consider a system of size $N_x \times N_y$ with periodic boundary conditions and look for small amplitude solutions in the presence of a uniform flow [for given values of ρ and $\mathbf{V} = (V_x,\ V_y) = \mathbf{J}/\rho$]. For a wave vector $\mathbf{k}$ in the reciprocal space of the computational domain, we search for solutions

$$f_\alpha(\mathbf{r}, t) \propto \exp(-i\mathbf{k}\cdot\mathbf{r} + zt). \tag{10}$$

To first order in $\mathbf{k}$, we have the linearized dispersion equation,

$$\det(\mathsf{K}^{(1)} + \mathsf{M}^{-1}\mathsf{C}\mathsf{M} - z\mathsf{I}) = 0, \tag{11}$$

where I is the identity operator, $\mathsf{K}^{(1)}$ is the linearized advection operator which is a diagonal matrix

$$\mathsf{K}^{(1)} = \mathrm{diag}(0,\ i\mathbf{k}\cdot\mathbf{e}_1,\ \ldots,\ i\mathbf{k}\cdot\mathbf{e}_8), \tag{12}$$

and C is the linearized collision operator

$$\mathsf{C} = \begin{pmatrix}
0 & 0 & 0 & 0 & 0 & 0 & 0 & 0 & 0 \\
\alpha_4 s_2 & -s_2 & 0 & 6V_x s_2 & 0 & 6V_y s_2 & 0 & 0 & 0 \\
\alpha_3 s_3/4 & 0 & -s_3 & 0 & 0 & 0 & 0 & 0 & 0 \\
0 & 0 & 0 & 0 & 0 & 0 & 0 & 0 & 0 \\
0 & 0 & 0 & c_1 s_5/2 & -s_5 & 0 & 0 & 0 & 0 \\
0 & 0 & 0 & 0 & 0 & 0 & 0 & 0 & 0 \\
0 & 0 & 0 & 0 & 0 & c_2 s_7/2 & -s_7 & 0 & 0 \\
\alpha_5 s_8 & 0 & 0 & 6a^2 V_x s_8 & 0 & -6V_y s_8/a^2 & 0 & -s_8 & 0 \\
0 & 0 & 0 & V_y s_9 & 0 & V_x s_9 & 0 & 0 & -s_9
\end{pmatrix}, \tag{13}$$

where

$$\alpha_4 = 2\left[3c_s^2 - (1 + a^2)\right], \tag{14a}$$

$$\alpha_5 = \frac{(1 - a^2)}{a^2}\left[2a^2 - 3c_s^2(a^2 + 1)\right]. \tag{14b}$$

The linearized dispersion equation (11) can be solved by perturbation technique in power series of $\mathbf{k}$ [8]. To ensure isotropy and Galilean invariance in the limit of $\mathbf{k} \to \mathbf{0}$, we need to solve the linearized dispersion equation up to $\mathbf{k}^2$.

In the first order of $\mathbf{k}$, three solutions are obtained: one corresponds to transverse excitations which are convected with the uniform speed of the fluid $\mathbf{k}\cdot\mathbf{V}/k$, whereas the other two are acoustic waves with phase velocity $\pm c_s$, where the speed of sound c_s can be chosen within limits that is deferred to later discussion. The sound waves also have the correct dependence on the applied uniform velocity $\mathbf{V}$ of the fluid up to first order in V,

i.e., $c_s \to c_s \pm V\cos\phi$, where ϕ is the angle between $\mathbf{k}$ and $\mathbf{V}$. The nonlinear terms in the equilibria of Eqs. (7a)–(7f) provide the correct Galilean coefficients for both transverse and longitudinal waves.

In the second order (in $\mathbf{k}$) of the solutions of the dispersion equation, the constraints on the isotropy of the transport coefficients for the hydrodynamic modes lead to

$$c_1 = \frac{c_2 + 4(1-a^2)}{a^2} \tag{15}$$

and the following relationships between the relaxation parameters

$$\frac{1}{\tilde{s}_2} = \frac{2(4+c_2)\left[\left(12c_s^2 - c_2\right)(1+a^2) - 2(5a^2+2)\right]}{(1+a^2)(1+c_2-3a^2)\left(c_2+10-12c_s^2\right) + 6[a^4(c_2-2) - 3(a^2-1)]}\frac{1}{\tilde{s}_9}, \tag{16a}$$

$$\frac{1}{\tilde{s}_8} = \frac{2(4+c_2)\left[\left(12c_s^2 - c_2\right)(1+a^2) - 2(3a^4+5a^2+5)\right]}{(1+a^2)(1+c_2-3a^2)\left(c_2+10-12c_s^2\right) + 6[a^4(c_2-2) - 3(a^2-1)]}\frac{1}{\tilde{s}_9}, \tag{16b}$$

where $1/\tilde{s}_\alpha \equiv (1/s_\alpha - 1/2)$. The coupling between s_2 and s_9 is required only when $a \neq 1$. The kinematic shear viscosity ν and the kinematic bulk viscosity ζ are

$$\nu = \frac{4+c_2}{6}\left(\frac{1}{s_9} - \frac{1}{2}\right), \tag{17a}$$

$$\zeta = \frac{1}{12}\left(7 + 3a^2 + c_2 - 12c_s^2\right)\left(\frac{1}{s_2} - \frac{1}{2}\right). \tag{17b}$$

For a given a, the speed of sound and c_2 must be chosen such that the shear and bulk viscosities are positive and the Eqs. (16a) and (16b) lead to positive values for s_2 and s_8.

The values of c_s and c_2, which optimize the isotropy and stability of the model, depending on the grid aspect ratio a, are determined by the linear analysis of the model [8]. In the case of square grid, i.e., $a = 1$, we have found $c_s^2 = 1/3$ and $c_2 = -2$. This result coincides with the one given in [8] and the relationship between s_8 and s_9 given by Eq. (16b), and the shear and bulk viscosities given by Eqs. (17a) and (17b), all reduce to the previous results for a square lattice where $c_1 = -2$ [see Eqs. (40)–(43) in [8] for c_s, $s_9(s_8)$, ν, and ζ, respectively]. However, the coupling between s_2 and s_9 is unique to the model on a rectangular grid. This coupling is due to the dependence of $p_{xx}^{(\mathrm{eq})}$ on ρ, which in turn leads the term $\alpha_5 s_8$ in the linearized collision operator C in Eq. (13). Finally, note that α_3 has little influence and is set to be equal to -2.

The linearized dispersion equation can be solved numerically for any value of $\mathbf{k}$ to determine the linear stability of the system by computing the rate of growth of spatially periodic excitations superimposed to a uniform flow of constant velocity $\mathbf{V}$, as previously shown in the case of a square grid [8]. Through this analysis it is found that the present model is much less stable than the square one, i.e., the stable region in parameter space of V and s_α is much smaller than that for the model with a square lattice. For instance, when $a = 1/2$, a stability condition is that $V \leq 0.05$, whereas for the model with a square lattice ($a = 1$), the same stability condition is that $V \leq 0.20$. One reason for this is that in general the sound speed c_s decreases with the aspect ratio a; for instance, when $a = 1/2$ the optimal speed of sound is about 0.377, which is different from the usual $c_s = 1/\sqrt{3} \approx 0.577$ on a square lattice. Therefore, the local velocity magnitude must be decreased accordingly

to keep the local Mach in check so that the low Mach number approximation remains valid. This means that the present model will have limited ability to simulate flows even at moderate Reynolds numbers. In addition, when using a combination of rectangular and square grids (the simplest case of grid refinement in one direction) in the situation where acoustic propagation is important, it will not be possible to choose an optimal value of the sound speed for the two different grids.

We would like to note that, although there is no simple interpretation of the instability of the LBE models because of the presence of a uniform velocity **V**, information on the instability can be obtained by analyzing the velocity dependence of the attenuation of sound waves using the linearized dispersion equation [8].

Let us consider the case where the uniform velocity is parallel to the wave vector **k** with a polar angle θ (between **k** and x-axis). For small values of k and the particular choice of c_2

$$c_2 = (a^2 - 3), \tag{18}$$

we have the following results. The transverse mode has phase velocity $v_\perp = V$ and its attenuation is given by

$$\gamma_\perp = k^2 \left(\frac{1}{s_9} - \frac{1}{2}\right)\left(\frac{(1+a^2)}{6} - V^2\left\{1 - \frac{9(1-a^2)^2 \sin^2 2\theta}{2\left[1 - 13a^2 + a^4 + 6(1+a^2)c_s^2\right]}\right\}\right). \tag{19}$$

For the longitudinal modes, we obtain as phase velocity $v_\parallel = \pm\sqrt{c_s^2 + V^2}$ and attenuation coefficient $\gamma_\parallel = (\gamma_b + \gamma_\perp)/2$, with (to first order in V)

$$\begin{aligned}\gamma_b = k^2 \left(\frac{1}{s_2} - \frac{1}{2}\right)\Bigg(&\frac{1 + a^2 - 3c_s^2}{3} \pm \frac{V}{c_s\left[1 + 8a^2 + a^4 - 12(1+a^2)c_s^2\right]} \\ &\times\left\{(1+a^2)\left(7a^2 + 36c_s^4\right) - 3\left(7 + 12a^2 + 3a^4\right)c_s^2\right. \\ &\left. + 12(1-a^2)c_s^2 \cos^2\theta\,[2 + (1-a^2)(2 - 3\cos^2\theta)]\right\}\Bigg).\end{aligned} \tag{20}$$

Contrary to the case of square grid, it is not possible in general with a given value of $a \neq 1$ to find a value of c_s for which the linear dependence of the attenuation of acoustic waves on V can be eliminated (for $a = 1$, this can be accomplished by setting $c_s^2 = 1/3$). This is a possible cause of instability in the model.

4. SIMULATIONS

We use the two-dimensional multirelaxation LBE model on either a square grid or a rectangular grid for the following simulations. The central routine (collision and advection) is quite close to that for the standard square LBE and leads to similar performances (using a workstation with a 500 MHz EV6 processor, the overall computation time per node and per time step is in the range 0.2 to 0.4 microsecond depending whether the cache is large enough or not).

4.1. A Vortex Traveling with a Constant Velocity

To test the ability of the present LBE scheme to simulate a viscous flow, we consider the particular case of a simple vortex superimposed to a uniform flow of velocity **V**. We take as initial condition for the flow

$$\mathbf{u}_0(\mathbf{r},\ t=0) = \mathbf{V} + (y_0 - y,\ x - x_0)\,\omega_0 \exp[-(\mathbf{r}-\mathbf{r}_0)^2/R^2], \tag{21}$$

where $\mathbf{r}_0 = (x_0,\ y_0)$ is the initial position of the vortex center, and ω_0 and R characterize, respectively, the amplitude and the extent of the vortex. The evolution of the corresponding macroscopic flow is fairly simple: the center of the vortex travels with the velocity **V** and the maximum value of the vorticity (at the center $\mathbf{r}_0 + \mathbf{V}t$) decays in time as

$$\omega_{\max}(t) = \frac{R^4\omega_0}{(R^2+4\nu t)^2} = \frac{\omega_0}{(1+4t^*)^2}, \tag{22}$$

where $t^* \equiv \nu t/R^2$ is the dimensionless time.

The system size is $N_x \times N_y = 109 \times 109$, with a grid aspect ratio $a = 1/2$. The size of the vortex is $R = 6$. Values of other parameters are: $\alpha_2 = -3.5$, $\alpha_3 = 2.0$, $c_2 = -2.9$, and $s_8 = 1.8$, i.e., $\nu = 0.01018$ according to Eq. (17a). The results obtained by the LBE simulations with various conditions agree very well with the analytic solution of the flow for $V = 0$. However, when V increases there are departures from the simple result of Eq. (22) because of the dependence of the transport coefficients and g-factor on **V**, as discussed for the square grid in [8]. An example of such behavior is demonstrated in Fig. 2. Figure 2 shows two LBE simulation results of $\omega_{\max}$ as a function of dimensionless time $t^* \equiv \nu t/R^2$, with $\mathbf{V} = (0,\ 0)$ and $\mathbf{V} = (0.05,\ 0)$. Equation (22) is used to fit the data to obtain the viscosity. The results are $\nu = 0.9876\nu_0$ and $\nu = 0.8966\nu_0$ for $V_x = 0$ and $V_x = 0.05$, respectively, where ν_0 is given by Eq. (17a). There are two factors that contribute to the correction in the viscosity: the wave-number **k**-dependence and **V**-dependence of

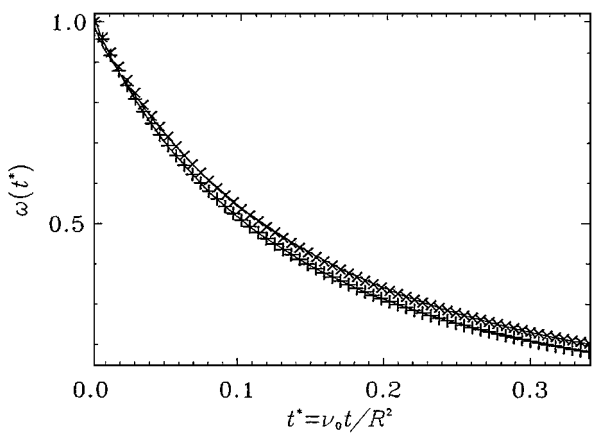

FIG. 2. LBE simulation of a moving vortex. Decay of the vorticity maximum. The grid aspect ration $a = 1/2$. Symbol $+$ and $\times$ are simulation results for $V = 0$ and $V = 0.05$, respectively. The solid lines are fitting of the data according to Eq. (22) with the viscosity of value $\nu = 0.9876\nu_0$ and $\nu = 0.8966\nu_0$, respectively, where ν_0 is given by Eq. (17a).

the transport coefficients [8]. The same simulations are performed on a square grid and the results are: $\nu = 0.9866\nu_0$ and $\nu = 0.8745\nu_0$ for $V_x = 0$ and $V_x = 0.05$, respectively. It should be noted that in the LBE simulations, initial conditions include not only the conserved quantities such as the density and velocity fields, but also all the nonconserved quantities such as fluxes and the stress, which can be obtained from the initial velocity field through a Chapman–Enskog analysis of the model.

4.2. Poiseuille Flow with Arbitrarily Inclined Walls

The second test is the two-dimensional Poiseuille flow with arbitrarily inclined walls. This situation allows us to test the no-slip boundary conditions in the LBE model. We consider a system of size $N_x \times N_y$ with periodic boundary conditions. The boundaries of the channel are placed with an arbitrary inclined angle θ with respect to x-axis, as illustrated in Fig. 3. The no-slip boundary conditions used here for the channel walls are the interpolated bounce-back boundary conditions proposed in [14]. The interpolated bounce-back boundary conditions combine interpolation and bounce-back schemes to deal with boundaries which are off the lattice points.

We first studied the time evolution of the flow starting at rest, and compared the results obtained by using the rectangular and square grids. The time evolution of velocity fields of the two systems agree very well with each other. We also studied the momentum transfer at the boundary. We found an excellent agreement between its measurements for the square and the rectangular grids, and its expected value: $\rho\nu L\partial_\perp V_\parallel$, where L is the length of the boundary, and $\partial_\perp V_\parallel$ is the normal derivative of the shear velocity with respect to the wall, computed at the wall.

Note that when we compute the momentum transfer for the rectangular grid, the components of the usual momentum transfer have to be multiplied by a factor a to account for the surface of the elementary cell (assuming that all results are in nondimensional units

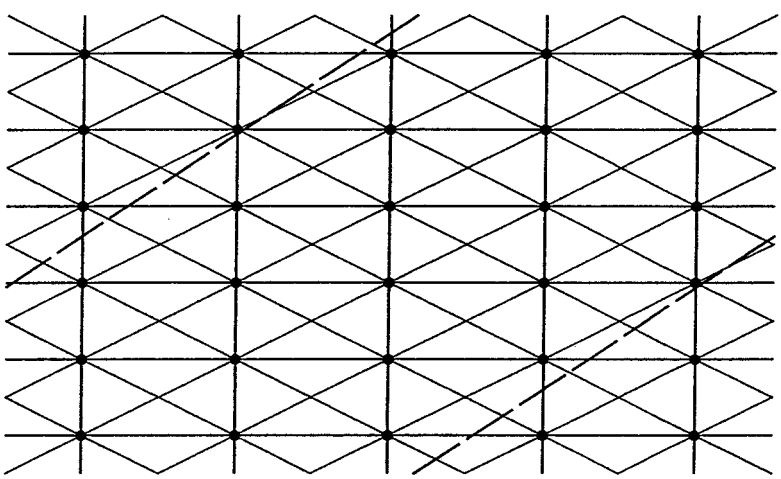

FIG. 3. 2D Poiseuille flow with arbitrary inclined walls. The system size is assumed to be $N_x \times N_y$. The discs are grid points. The solid lines are the advection lines of the discrete velocities. The dashed lines are the boundaries of the channel. The width of the channel is N_y. The no-slip boundary conditions are enforced at the intersections of the dashed lines and the thin solid lines.

defined on the square grid). In order to better understand the origin of this factor, one has to remember that ρ and **j** are the mass and momentum densities (mass and momentum per unit surface), while the momentum transfer has to be computed from momentum: (momentum density) $\times$ (cell surface). Usually a unique regular grid is used and the cell volume can be taken as unit volume. Here however the surface of the cells is equal to the chosen aspect ratio a once the square cell has been taken as unit surface. Indeed this remark applies to the next section when computing the drag and lift coefficients.

4.3. Flow Past a Cylinder Asymmetrically Placed in a Channel

The third test we did was a two-dimensional flow past a cylinder asymmetrically placed in a channel. This flow has been used as a standard benchmark test in CFD [15]. The flow configuration is as follows: a cylinder of diameter d is placed in a channel of width $4.1d$ and length $22d$, the center of the cylinder is asymmetrically (with respect to the center line of the channel) located at horizontally $2d$ from the entrance, and vertically $2d$ from the lower wall of the channel, as shown in Fig. 4. The boundary condition at the entrance is a Poiseuille profile with average speed U. The boundary condition at the exit is free exit with a total flux equal to the input flux. The bounce-back boundary conditions are used for the channel walls, and the interpolated bounce-back boundary conditions with a second-order interpolation [14] are used for the boundary of the cylinder. The Reynolds number for the flow is

$$\mathrm{Re} = \frac{Ud}{\nu}.$$

We use the LBE model to simulate the flow at $\mathrm{Re} = 100$ for which there is periodic vortex shedding behind the cylinder.

The flow was computed on rectangular grids with several different values of the grid aspect ratio a, and compared to the results with a square grid. The measured quantities are Strouhal number St, maximum drag $C_D^{\max}$, maximum lift coefficient $C_L^{\max}$, minimum lift coefficient $C_L^{\min}$, and the pressure difference ΔP. The results are summarized in Table I. Table I also shows the lower and upper bounds of St, $C_D^{\max}$, $C_L^{\max}$, and ΔP, obtained by a number of conventional CFD methods presented in [15]. Overall, the LBE simulation results with square or rectangular grids agree well with each other, and with the CFD results in [15]. Figure 5 shows the contours of the stream function $\psi(x, y)$ and the vorticity $\omega(x, y)$ of the simulations on a square grid of size $N_x \times N_y = 1401 \times 308$ and on a rectangular grid of size $N_x \times N_y = 1401 \times 616$. The relative L^2-norm difference of the two velocity fields is about 2.2×10^{-4}. Note that the aspect ratio for this particular calculation is slightly

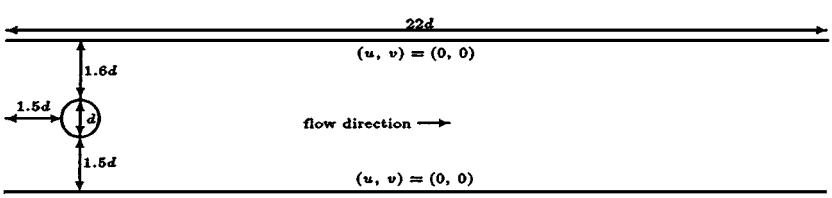

FIG. 4. Configuration of a 2D flow past a cylinder asymmetrically placed in a channel.

TABLE I

2D Flow Past a Cylinder Asymmetrically Placed in a Channel at Re = 100

a	c_s	c_2	$N_x \times N_y$	St	$C_D^{\max}$	$C_L^{\max}$	$C_L^{\min}$	ΔP
1.00	$1/\sqrt{3}$	-2	709×132	0.3021	3.153	0.926	-1.018	2.50
0.85	0.6141	-0.80	709×155	0.3018	3.186	0.984	-1.051	2.51
0.80	0.5829	-0.90	709×165	0.3020	3.174	0.950	-1.062	2.51
0.75	0.5412	-1.10	709×176	0.3018	3.173	0.965	-1.053	2.51
0.70	0.5113	-1.50	709×188	0.3007	3.195	1.013	-1.071	2.51
0.65	0.4761	-1.70	709×203	0.3009	3.184	0.999	-1.062	2.47
0.60	0.4417	-2.00	709×220	0.3009	3.176	1.002	-1.053	2.45
0.55	0.4086	-2.25	709×240	0.3015	3.189	1.005	-1.052	2.42
0.50	0.3770	-2.55	709×264	0.3007	3.199	1.019	-1.084	2.45
0.45	0.2977	-2.90	709×293	0.2992	3.204	1.053	-1.107	2.50
CFD lower bound in Ref. [15]				0.2950	3.22	0.99	—	2.46
CFD upper bound in Ref. [15]				0.3050	3.24	1.01	—	2.50

different from that shown in Fig. 4, but this has negligible effect for the present purpose of comparing results on the square and the rectangular grids.

The relative fluctuation of Strouhal number St is well under 1% and the values of St are well within the bounds in [15]. The fluctuation of $C_D^{\max}$ is also under 1% but the values of $C_D^{\max}$ are all slightly lower than the results in [15]. The fluctuation of ΔP is about 1% and the values of ΔP agree well with the results in [15]. The values of lift coefficient obtained by the LBE simulations have a variation about $\pm 6\%$, which is much greater than the variations in other measured quantities.

A possible origin of the discrepancy in the lift coefficients is the following. The LBE method is intrinsically a compressible scheme and acoustic waves may be generated by, e.g., initial conditions that do not include a proper pressure field or the flow itself that generates an oscillating pressure field as is the case considered here. For a given value of the sound speed and a given choice of the boundary conditions at the entrance and exit of the channel

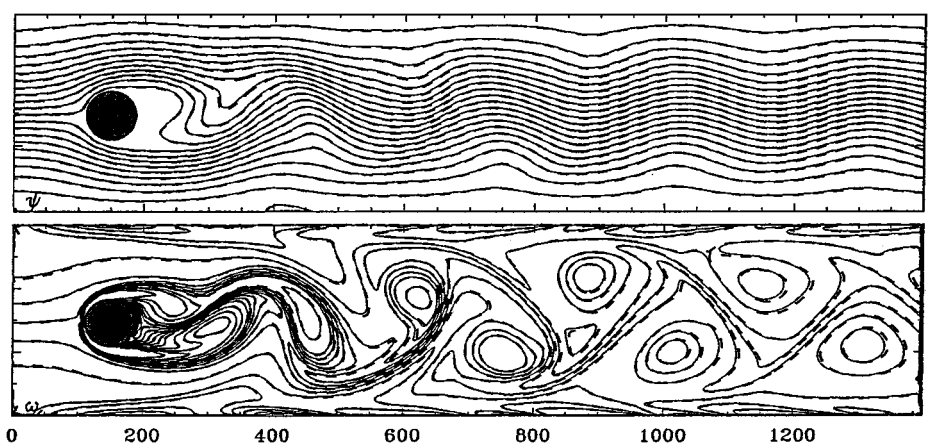

FIG. 5. 2D flow past a cylinder asymmetrically placed in a channel at Re = 100. Top and bottom figure show contours of the stream function $\psi(x, y)$ and the vorticity $\omega(x, y)$ of the flow, respectively. The dashed lines are the simulation results on a square grid of size $N_x \times N_y = 1401 \times 308$, and the solid lines are that on a rectangular grid of size $N_x \times N_y = 1401 \times 616$.

the frequency of some of the longitudinal acoustic modes can be close to multiples of the Strouhal frequency in the flow. This causes resonances between some of the acoustic waves and the periodic shedding of vortices by the cylinder. The coupling between acoustic waves and vortex shedding indeed affects the hydrodynamic fields, and in turn, various measured quantities. Among the measured quantities, the lift coefficients are most sensitive to this effect. The mean drag coefficient is also affected but to a much smaller extent. This problem is of broad interest. However, it will be easier to study it with the model of square grid for which the speed of sound and the bulk viscosity can be chosen in a broader range than for the model of rectangular grid. A detailed study is beyond the scope of the present work and will be addressed elsewhere.

5. CONCLUSION AND DISCUSSION

In this paper we have successfully proposed a two-dimensional nine-velocity generalized lattice Boltzmann model with multiple relaxations on a rectangular grid with arbitrary aspect ratio $a = \delta_y/\delta_x$. We have numerically validated the model by using the model to simulate several benchmark problems, and have obtained satisfactory results. In contrast to the previous two-dimensional, nine-velocity, multirelaxation model on a square grid [8], the model on a rectangular grid is more prone to instability, and the admissible maximum value of local velocity magnitude is much less than that in the model on a square grid. It should also be stressed that, although this work is in part motivated by a previous work [2], it is realized that the nine-velocity lattice BGK equation cannot possibly work properly on a rectangular grid. Specifically, the lattice BGK equation does not have sufficient degrees of freedom to satisfy the constraints imposed by isotropy and Galilean invariance. With nine discrete velocities in two dimensions, it is necessary to use the multirelaxations to construct an LBE model on a rectangular grid.

This work is our first attempt to construct a lattice Boltzmann model on an arbitrary unstructured grid. As discussed in Ref. [9], one difficulty encountered in the LBE model on an unstructured grid is due to the fact that $\nabla \mathbf{e}_\alpha f \neq \mathbf{e}_\alpha \nabla f$ because the discrete velocity set $\{\mathbf{e}_\alpha\}$ has spatial dependence. In this work, we found that there are additional issues in the LBE model on an unstructured grid needed to be addressed.

First, we found that the local grid structure severely affects the local sound speed. If the sound speed varies spatially depending on local grid structure, then the model is unphysical. Correct acoustic propagation is an essential part of the lattice Boltzmann method. Secondly, the constraints of isotropy and Galilean invariance are difficult to satisfy by using the lattice BGK model, as proposed in [9], unless the discrete velocity set includes a large number of velocities. Thirdly, the numerical stability is severely affected by the local grid structure even for uniform structured grid, as we have demonstrated in this work. Stability is of key importance to an effective lattice Boltzmann algorithm. However, we have not yet developed a method to systematically improve the stability of the lattice Boltzmann method. We believe that the aforementioned issues must be resolved before we can construct a lattice Boltzmann model on an arbitrary unstructured grid.

ACKNOWLEDGMENTS

D.d'H. and P.L. acknowledge the support from ICASE for their visit to ICASE in 1999–2000, during which part of this work was performed. L.S.L. acknowledges partial support from NASA Langley Research Center under

the program of Innovative Algorithms for Aerospace Engineering Analysis and Optimization. The authors thank Dr. M. Salas, the director of ICASE, for his support and encouragement of this work.

REFERENCES

1. D. d'Humières, Generalized lattice-Boltzmann equations, in *Rarefied Gas Dynamics: Theory and Simulations, Progress in Astronautics and Aeronautics*, edited by B. D. Shizgal and D. P Weaver, (AIAA Press, Washington, DC, 1992), Vol. 159, pp. 450–458.
2. J. M. V. A. Koelman, A simple lattice Boltzmann scheme for Navier–Stokes fluid flow, *Europhys. Lett.* **15**, 603 (1991).
3. U. Frisch, B. Hasslacher, and Y. Pomeau, Lattice-gas automata for the Navier–Stokes equation, *Phys. Rev. Lett.* **56**, 1505 (1986).
4. X. He and L.-S. Luo, A priori derivation of the lattice Boltzmann equation, *Phys. Rev. E* **55**, R6333 (1997); Theory of the lattice Boltzmann method: From the Boltzmann equation to the lattice Boltzmann equation, *Phys. Rev. E* **56**, 6811 (1997).
5. T. Abe, Derivation of the lattice Boltzmann method by means of the discrete ordinate method for the Boltzmann equation, *J. Comput. Phys.* **131**, 241 (1997).
6. X. He and G. D. Doolen, Lattice Boltzmann method on a curvilinear coordinate system: Vortex shedding behind a circular cylinder, *Phys. Rev. E* **56**, 434 (1997); Lattice Boltzmann method on curvilinear coordinates system: Flow around a circular cylinder, *J. Comput. Phys.* **134**, 306 (1997).
7. O. Filippova and D. Hänel, Grid refinement for lattice-BGK models, *J. Comput. Phys.* **147**, 219 (1998).
8. P. Lallemand and L.-S. Luo, Theory of the lattice Boltzmann method: Dispersion, dissipation, isotrophy, Galilean invariance, and stability, *Phys. Rev. E* **61**, 6546 (2000).
9. I. V. Karlin, S. Succi, and S. Orszag, Lattice Boltzmann method for irregular grids, *Phys. Rev. Lett.* **82**, 5245 (1999).
10. Y. H. Qian, D. d'Humières, and P. Lallemand, Lattice BGK models for Navier–Stokes equation, *Europhys. Lett.* **17**, 479 (1992).
11. H. Chen, S. Chen, and W. H. Matthaeus, Recovery of the Navier–Stokes equations using a lattice-gas Boltzmann method, *Phys. Rev. A* **45**, R5339 (1992).
12. We noted that although the model in Ref. [2] proposed to use face-centered rectangular grid, only the square grid was used in the numerical tests in Ref. [2].
13. X. He and L.-S. Luo, Lattice Boltzmann model for the incompressible Navier–Stokes equation, *J. Stat. Phys.* **88**, 927 (1997).
14. M. Bouzidi, M. Firdaouss, and P. Lallemand, Momentum transfer of a lattice-Boltzmann fluid with boundaries, *Phys. Fluids* Submitted for publication.
15. M. Schäfer and S. Turek, Benchmark computations of laminar flow around a cylinder, in *Notes in Numerical Fluid Mechanics* (Vieweg Verlag, Braunschweig, 1996), Vol. 52, pp. 547–566.